Icarus 203 (2009) 242–249

Contents lists available at ScienceDirect

Icarus

journal homepage: www.elsevier.com/locate/icarus

Determining a tilt in Titan's north–south albedo asymmetry from Cassini images

Michael T. Roman [a,*], Robert A. West [b], Donald J. Banfield [a], Peter J. Gierasch [a], Richard K. Achterberg [c], Conor A. Nixon [c], Peter C. Thomas [a]

[a] Department of Astronomy, Cornell University, Ithaca, NY 14853, USA
[b] MS 169-237, Jet Propulsion Laboratory, 4800 Oak Grove Drive, Pasadena, CA 91109, USA
[c] Department of Astronomy, University of Maryland, College Park, MD 20742, USA

ARTICLE INFO

Article history:
Received 11 October 2008
Revised 30 March 2009
Accepted 13 April 2009
Available online 13 May 2009

Keywords:
Titan
Atmospheres, dynamics
Atmospheres
structure

ABSTRACT

Analysis of Titan's hemispheric brightness asymmetry from mapped Cassini images reveals an axis of symmetry that is tilted with respect to the rotational axis of the solid body. Twenty images taken from 2004 through 2007 show a mean axial offset of 3.8 ± 0.9° relative to the solid body's pole, directed 79 ± 24° to the west of the sub-solar longitude. These values are consistent with recent measurements of an implied atmospheric spin axis determined from isothermal mapping by [Achterberg, R.K., Conrath, B.J., Gierasch, P.J., Flasar, F.M., Nixon, C.A., 2008. Icarus 197, 549–555].

1. Introduction

Since first being resolved nearly three decades ago, the atmosphere of Titan has been observed to exhibit a distinct variation in albedo from south to north. The observations from Voyagers 1 and 2 in the early 1980s, near the time of Titan's northern vernal equinox, showed the northern hemisphere to have a significantly lower albedo than the southern hemisphere when viewed through green, blue, and violet filters (Sromovsky et al., 1981; Smith et al., 1981). A decade later, well into the northern summer solstice of Titan's 29.5-year-long orbit, HST observations by Caldwell et al. (1992) revealed a reversal in the albedo asymmetry. Often termed the north–south asymmetry (hereafter NSA), this feature has been observed to display a seasonal dependence that reveals the importance of solar heating in shaping the chemistry and dynamics of Titan's atmosphere (see Lorenz et al., 1997).

Examining Voyager 1 images, Sromovsky et al. (1981) found the NSA to be nearly axially symmetric, though definite longitudinal variations were observed; for example, the north polar zone boundary was noted as being slightly inclined relative to latitude lines. Recent analysis of thermal maps assembled from observations made by Cassini's Composite Infrared Spectrometer (CIRS) also shows an offset, implying that the spin axis of this atmospheric mean zonal flow is tilted with respect to the solid body pole (Achterberg et al., 2008b; see Flasar et al., 2004, for information on the CIRS instrumentation). Analyzing data collected from July of 2004 through May of 2007, Achterberg et al. (2008b) measured an amplitude and phase of longitudinal thermal structure corresponding to dominant wavenumber 1. Interpreted as an offset of the rotational axis of the atmosphere relative to Titan's IAU defined pole (Seidelmann et al., 2007), they found it to be inclined by 4.1 ± 0.2° with an azimuth orientation of 76 ± 2° from the sub-solar longitude.

Study of this tilt may provide insight into the complex atmospheric dynamics of Titan. Implied pressure gradients from Voyager IRIS measurements suggest that Titan's atmosphere is rotating at a rate substantially greater than the solid body beneath (Flasar et al., 1981; Flasar and Conrath, 1990), and measurements from several sources have supported this conclusion (e.g. Sicardy et al., 1999; Kostiuk et al., 2001). While such atmospheric superrotation is also observed on Venus, Titan's larger inclination with respect to the Sun's orbital plane may provide an opportunity to observe the effects of varying insolation on such a system. The orientation of the atmospheric tilt is presumably indicative of the dynamical processes involved, and measurements of its value may help to evaluate theory and constrain atmospheric models.

Though the atmosphere of Titan appears nearly featureless, it is not unreasonable to suspect that the dominant feature—the NSA—may visually express evidence of the dominant large-scale atmospheric circulation. Just as hints of a visual tilt were noted in Voyager images, here we presumed that it would be possible to detect and measure a possible offset of the NSA in images from Cassini.

* Corresponding author. Address: Department of Astronomy, Cornell University, 311 Spaces Sciences Building, Ithaca, NY 14853, USA.
E-mail address: mtroman@astro.cornell.edu (M.T. Roman).

0019-1035/$ - see front matter © 2009 Elsevier Inc. All rights reserved.
doi:10.1016/j.icarus.2009.04.021

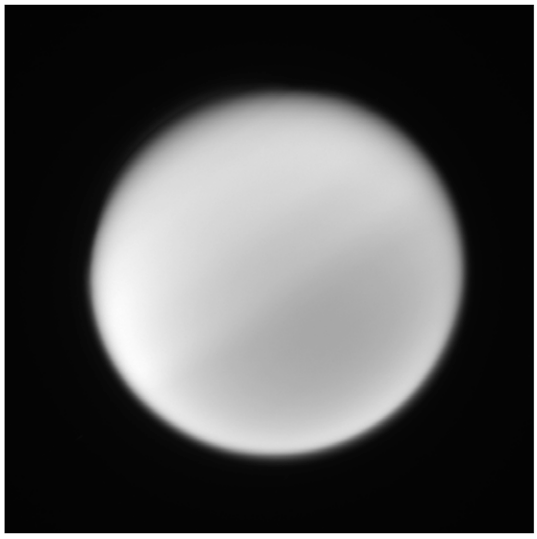

Fig. 1. Image N1562038525, photometrically calibrated. The image has been scaled to reveal the albedo contrast of the NSA.

Such measurements would serve as an independent visual compliment to the CIRS thermal measurements, and so it is with this motivation that Cassini images of Titan from 2004 through 2007 are here investigated.

2.1. Observations, processing and analysis

Criteria for image selection were based on image filter, spatial and temporal resolution, and target viewing geometry. Images were collected from both the Cassini Narrow Angle Camera (NAC) and Wide Angle Camera (WAC). Each image was taken through an 890 nm methane filter (MT3), which clearly emphasized the NSA contrast, with phase angles (Sun–Titan-observer) sufficiently low enough (generally less than 30°) to display a majority of Titan's disc (see Fig. 1). Since our analysis required careful brightness measurements and accurate navigation, it was necessary that Titan's disc appeared large enough (generally greater than 300 pixels in diameter) to adequately define the detached haze layer, but small enough to amply fit a majority within the frame of the image. With these requirements in mind, images were selected to sample the greatest time span possible. Occasional temporal groupings (i.e. several taken from the same day), were analyzed when available to help verify the consistency of our measurements, assuming that any large-scale physical variance would exist on time scales greater than a day. In all, 20 photometrically calibrated Cassini images were selected for analysis, dating from October 2004 to 2007. Data about the images and relevant geometries are provided in Table 1. Comprehensive data about the Cassini imaging instruments can be found in Porco et al. (2004).

Each image was navigated using a limb fitting routine[1] to determine the correct planet center camera pointings. The initial pointings based on post-fly-by reconstructed values proved inadequate, as was evident due to obvious visual inconsistencies between consecutive mapped images. The outer detached haze of the disk was fitted assuming a spherical body of radius 3100 km, accounting for Titan's thick atmosphere; this value was based on the least-squares goodness of fit for a circle fit to the location of peak brightness within the haze layer (see Fig. 2). Analysis shows that the detached haze layer is nearly spherical and well centered about Titan; Achterberg et al. (2008a) showed that the atmospheric rotation decays with height above 250 km of elevation and is quite small at 500 km, consistent with a spherical isobaric surface. Additionally, since the detached haze extends several hundred kilometers above the opaque lower haze, a greater portion of the detached haze remains illuminated at relatively high phase angles, allowing greater constraint on our fits. The resulting planet center pointings were determined to be accurate to within one pixel.

The images were then calibrated using CISSCAL (Cassini Imaging Science Subsystem Calibration) software and cleaned to remove obviously bad pixels, imaging artifacts and significant noise, replacing outliers with surrounding means. Using the geometric data and newly calculated camera center pointings, the images were mapped onto simple cylindrical projections using the MaRC[2] mapping software. A map resolution was chosen based on the spatial resolution of the original image, which resulted in map resolutions ranging from slightly less than 0.2° per pixel to 0.5° per pixel. The IAU defined north pole of Titan's solid body, defined as having a right ascension of 36.41° and declination of 83.94° (Seidelmann et al., 2007), was used to determine north (up) in the mapped projection (see Fig. 3). It should be noted that Stiles et al. (2008) determined a different north pole using Cassini RADAR images; they report a right ascension of 39.48° and a declination of 83.43°, which results in a 0.61° change in north azimuth angle and an approximately 3° increase in sub-solar longitude. Since Achterberg et al. (2008b) used the Seidelmann et al. (2007) defined spin values for their analysis, we likewise chose to use these same values for consistency.

Finally, it was necessary to choose an effective radius at which to map the images. In the case of a clearly defined surface layer, the effective radius would easily be defined by the clearly delineated radius of the solid body (i.e. from target center to limb in image space); given the precise boundaries of the target, the mapping software can then produce a projection with accurately defined coordinates. However, in this study, we examined the hazy atmosphere of Titan, of which the correct radius was less certain. Furthermore, since we intended to measure the NSA, the correct value depended on the height of the cloud layer in which the contrast was manifested. Since the contrast was presumably produced in an extended diffuse layer, defining it at a discrete height was physically inaccurate, but unfortunately necessary for the mapping process. The value of this height was not well constrained, but analysis indicates that the contrast was produced by differences in the stratospheric haze above 80 km in altitude (M. Tomasko, R.West, personal communication); therefore, we chose to map the cloud height at 80 km and attempted to account for the significant uncertainty in our error calculations.

With the images carefully mapped, we turned to our goal of best determining the latitude of an imposed line delineating the high and low albedo regions (roughly north and south hemispheres, respectively) for the purpose of quantifying the apparent difference in orientation between the pole vectors of the solid body and super-rotating atmosphere.

In a mapped image of Titan, it was presumed that the NSA could be characterized by a profile depicting brightness as a function of latitude for any given longitude, in which consistently high brightness values at high latitudes would begin to gradually diminish over a finite width near the equator until reaching steady values of relatively lower brightness at southern latitudes. A profile of this brightness gradient between the contrasting albedos could presumably be modeled simply by a curve of a hyperbolic tangent,

[1] The routine, NAV, is part of the Video Image Communication And Retrieval (VICAR) software, developed primarily at the Jet Propulsion Laboratory over the last several decades.

[2] MaRC (Map Reprojections and Conversions) is a free C++ library and program developed by Ossama Othman to produce map projections. Further information and software can be found at http://sourceforge.net/projects/marc/

Table 1
The images used for this analysis, listed in chronological order along with relevant observing geometries. Image names beginning with *N* indicate the images were taken with the Narrow Angle Camera (NAC); *W* indicates the Wide Angle Camera (WAC). North Clock Angles are measured clockwise from top-center of the image.

Image name	Image mid time (yyyy,ddd,hh,mm,ss,mmm)	Target distance (km)	Target sub-solar latitude	Target sub-solar longitude (W)	Target sub-spacecraft latitude	Target sub-spacecraft longitude (W)	Target north clock angle
N1477225220	2004,297,11,54,19,886	1790628	−23.5°	88.6°	−12.4°	110.0°	90.1°
N1481448770	2004,346,09,06,29,396	1120207	−23.1°	110. 4°	−9.1°	122.7°	38.5°
W1487123242	2005,04,60,12,04,2442	114072	−22.5°	150. 6°	−2.7°	154.0°	10.3°
N1496569460	2005,155,09,16,05,950	1239799	−21.1°	94. 8°	−27.1°	103.3°	125.6°
N1496574260	2005,155,10,36,05,920	1213312	−21.1°	96. 1°	−27.7°	104.1°	129.8°
N1496579060	2005,155,11,56,05,890	1186939	−21.1°	97. 3°	−28.3°	104.9°	134.2°
N1496583860	2005,155,13,16,05,860	1160691	−21.1°	98. 6°	−28.9°	105.7°	138.5°
W1509139296	2005,300,20,52,51,612	148638	−19.8°	133. 8°	−0.4°	140.1°	32.9°
W1509148861	2005,300,23,32,16,551	95235	−19.8°	136. 3°	−0.4°	150.4°	35.0°
W1514292901	2005,360,12,25,27,611	131387	−19.1°	38. 3°	−0.1°	18.6°	315.4°
N1557906451	2007,135,07,13,16,220	1287508	−12.2°	257.2°	13. 1°	255.3°	355.6°
W1559103294	2007,149,03,40,34,593	185954	−12.1°	209.4°	10. 2°	216.6°	17.9°
N1559283948	2007,151,05,51,24,490	1294884	−12.0°	256.7°	8. 0°	254.7°	354.4°
W1561882135	2007,181,07,34,23,020	310610	−11.5°	214.6°	0. 1°	215.6°	360.0°
W1561882245	2007,181,07,36,01,030	311199	−11.5°	214.6°	0. 1°	215.6°	360.0°
W1561882355	2007,181,07,37,51,030	311861	−11.5°	214.6°	0. 1°	215.6°	360.0°
N1562038525	2007,183,03,00,44,040	1314553	−11.5°	255.4°	0. 0°	248.1°	328.1°
N1567440863	2007,245,15,39,07,810	1318627	−10.6°	225. 0°	−3.3°	243.9°	359.8°
N1570187018	2007,277,10,28,05,430	1228641	−10.1°	221.5°	2. 1°	245.4°	62.3°
N1570187128	2007,277,10,29,51,430	1229364	−10.1°	221.5°	2. 1°	245.4°	62.3°

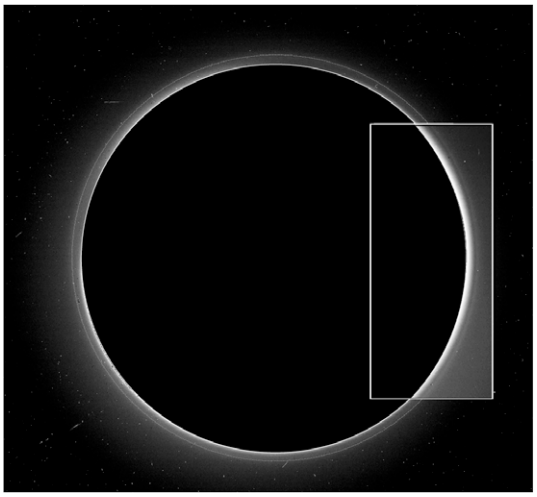

Fig. 2. Fitting the detached haze. Each image was scaled to accentuate the gentle contrast of the detached outer haze before running VICAR's NAV routine to determine the best fit. The insert clearly shows the detached outer haze as a faint, concentric ring extending above the denser stratospheric haze. A circle of radius 3100 km was then fit to the spherical detached haze layer to determine the camera center pointings for Titan in the image.

or possibly a cubic function, whose inflection point would serve to mark the NSA boundary; however, in practice, attempts to determine the location of the inflection points in fits to the data proved unsuccessful as the gradual gradient in signal was often overwhelmed by noise and physical variation that served to deviate the profile from the simple underlying hyperbolic tangential form.

In order to overcome this variability and yet still make use of the basic trend in brightness, a more robust method was employed. Each mapped image was shifted in latitude and subtracted against itself (two identical 'layers' one shifted up, the other down), so that a latitudinal difference in brightness between the two layers was mapped. In regions where the latitudinal brightness gradient was nearly zero, the difference was nearly zero (i.e. high albedo *cancelled* high albedo, and low albedo *cancelled* low albedo). Oppositely, in regions of greater latitudinal albedo gradient, where the small change in latitude would cause a pronounced difference in brightness, the magnitude of the difference between the overlaying shifted layers increased (i.e. the albedos no longer cancelled and high brightness values subtracted from lower brightness values resulted in greatly negative values—the basic idea can be illustrated by considering the difference between two identical hyperbolic tangents in Fig. 4). Thus the inherent albedo gradient within the mapped images was used to create an artificial minimum feature—a dark band of width equal to twice the amount shifted at the equatorial contrast region. It was assumed that the latitudes of greatest contrast would define the edges of this artificial band, so that the band will acquire a shape and orientation that mimics the actual NSA contrast boundary. It follows that the midpoint represents a realistic location at which to define the North South Asymmetry boundary.

The data was processed as described above, taking a difference between two copies of an image, each shifted 3° of latitude in opposite directions along the vertical axis. As desired, this created a dark band running more or less horizontally across the image, effectively delineating the boundary in albedo between the Northern and Southern hemispheres (see Fig. 5).

The region of interest is that within the equatorial region, and only the portion of that undistorted by possible limb foreshortening or brightening. This region was chosen to be defined as a portion of the map with latitudes between 25.0° S and 15.0° N, and with values of the cosine of the emission angles, μ, greater than 0.4 (corresponding to emission angles less than ∼66°). Columns of an array representing this selected region of the differenced map were then chosen and averaged over 2° wide bins centered at alternating degrees of longitude. The result was brightness as a function of latitude for discrete values of longitude, each displaying a prominent minimum region in the horizontal dark band.

If the meridional albedo variation followed a perfect hyperbolic tangent in form, it could be assumed that an absolute minimum would occur at the vertical midpoint of the entire minimum region; however, due to image noise and possible physical/meteorological variations, the curves are asymmetric and the absolute minimum and midpoint do not necessarily coincide. Considering this and the assumptions of the method employed, a polynomial function was fit to the minimum region for each of the longitude bins, and the location of the fit's minimum provided a robust measurement of the latitude at which the NSA can be delineated for that bin of longitude. These latitudinal values were calculated for

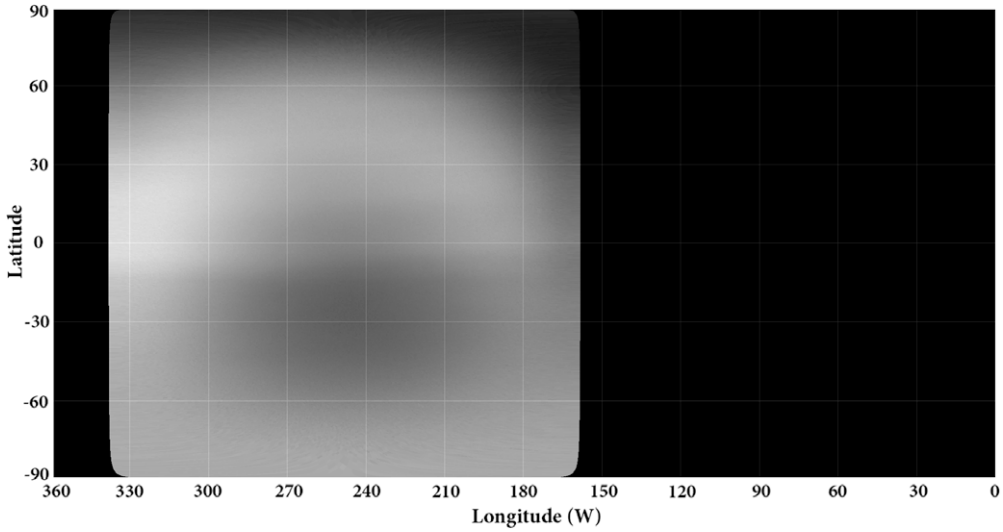

Fig. 3. Simple cylindrical projection of image N1562038525 with a superimposed grid of latitudes and west longitudes. Note the boundary between the low and high albedo regions defining the NSA just south of the equator.

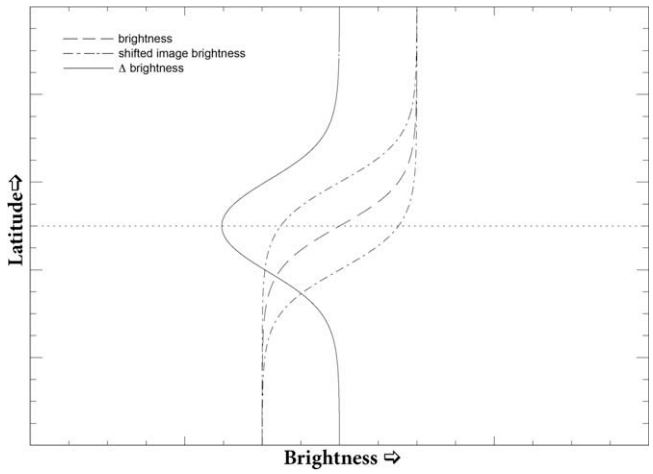

Fig. 4. Schematic representation of the method employed to demarcate the NSA. A hyperbolic tangent models brightness contrast. When shifted north and south, the difference between the two shifted curves produces a minimum in brightness centered at the inflection point of the original curve.

each longitudinal bin and then plotted as a function of west longitude.

If the NSA boundary were assumed to form a circle of constant latitude around Titan, no trend would be expected in the above plot; however, if the atmosphere were tilted with respect to the solid body, that is to say if the normal to this plane was not axially symmetric with the polar vector of Titan, the resulting boundary would show some trend. When mapped in a cylindrical projection, if the angle of tilt were sufficiently small and the boundary sufficiently close to the equator, it is assumed that the latitude would vary in an approximately sinusoidal manner. It follows that wavenumber 1 would have a wavelength of 360° of longitude and the amplitude will be equal to the deviation from axial symmetry. The longitudinal position of the minimum latitude of this curve will also indicate the longitudinal location of the northern pole of the NSA tilt axis.

With this reasoning, each set of data (latitude as a function of longitude) was fit to a sinusoidal function of the form $Lat\ (lon) = A\ sin(lon - lon_0) + lat_0$ using a least-squares fit method, with free parameters of amplitude A, a longitudinal shift in phase lon_0, and latitudinal offset lat_0 (see Fig. 6).

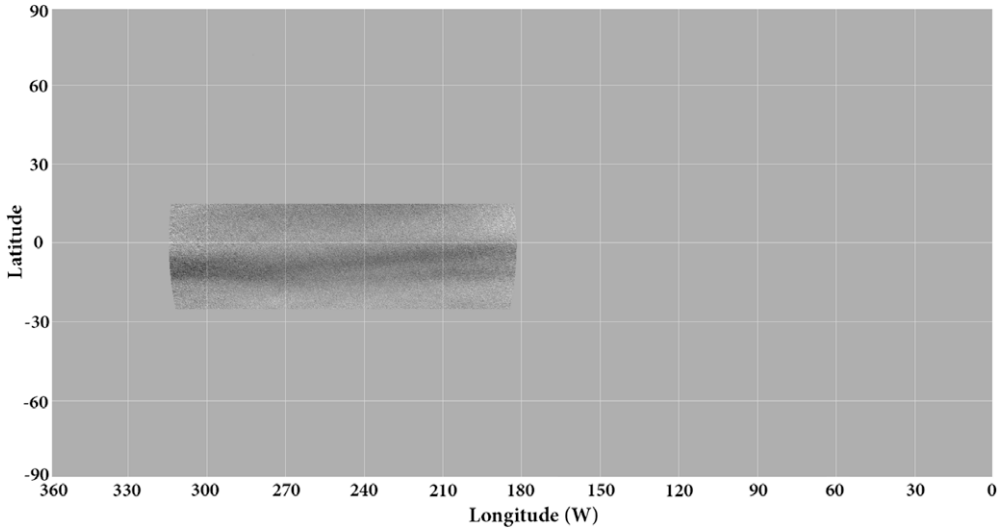

Fig. 5. A differenced image (N1562038525), clearly displaying the artificial minimum band that serves to demarcate the region of greatest contrast and represent the NSA boundary.

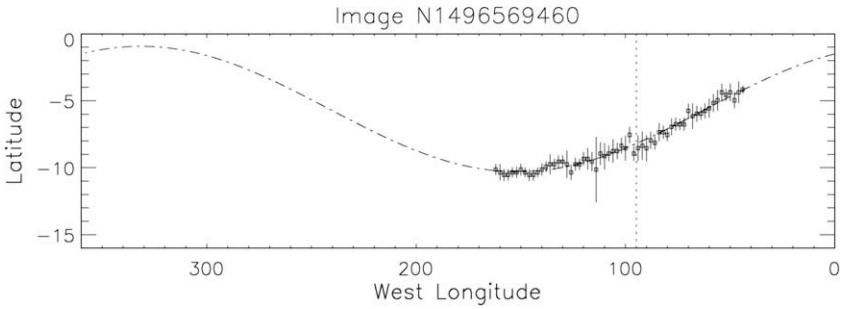

Fig. 6. Plot of the NSA boundary latitude as a function of longitude (N1496569460 is shown here as an example). Uncertainty in the determination of the boundary latitude is represented in the vertical error bars. The sub-solar longitude is represented by the vertical dotted line. Plots for the remaining set are depicted in Fig. 7.

2.2. Error analysis

In each step of the analysis, an attempt was made to carefully identify and account for the source and magnitude of the errors in measurements used to determine the values of the parameters in the above fitted function. Errors in the fit were combined with navigational uncertainty within the mapped projections to determine the accuracy with which we can report values of the NSA boundary and implied atmospheric tilt.

Assuming our model was correct, the fundamental sources of error in the fitting technique were due to the pixel resolution of the maps (~0.2° for NAC and ~0.5° for WAC images) and the random noise in brightness values that were used to determine the NSA latitudinal gradient profiles. When creating the mean latitude profiles of brightness at each longitude, we attributed the standard deviation as the error for each mean sample. When the bin was fitted, the data was weighed by these standard deviations, and the resulting one-sigma standard deviation (σ) of the fit parameter was added in quadrature to the pixelization error, providing a total σ_{bin} for the NSA boundary latitude at that bin of longitude. Cumulatively, this sigma expresses the uncertainty, due to random noise, pixelization, and physical variation, with which we can determine the midpoints of these fits and thus the latitude of greatest brightness gradient taken to define the NSA boundary for a given longitude.

Each NSA boundary latitude as a function of longitude was then least squares fit to the aforementioned sinusoidal function, with data weighted based on σ_{bin} for each value. The resulting standard deviations of the fitted parameters express the uncertainty in these parameters based on the previously determined uncertainty of the data being fitted.

In addition to the process of fitting the data, significant error was introduced due to an uncertainty in planet center pointings, which define where Titan is centered in the image, and the height of the NSA contrast, which determines the effective radius of the mapped body. Each of these uncertainties introduces an error in the absolute latitude and longitude of each mapped data point due to translational and projection effects in the mapped image. In an attempt to quantify these values, a simple Monte Carlo method was employed to estimate the possible error in the final results given the expected range in each parameter's uncertainty.

Planet center pointings were determined to have an uncertainty of less than one pixel. The height of the effective NSA contrast layer was less certain, so values ranging from 50 km greater than to

Table 2
The images, listed in chronological order, with NSA tilt parameters determined by our analysis. For each image, the first two columns present the image name along with the time at which it was taken (year, day of the year, hour of the day), respectively. The third column reports the magnitude of the offset of the atmospheric pole with respect to the solid body pole. The fourth column reports the azimuth orientation of this offset. The fifth column reports the mean latitude of the NSA. The final two columns provide the sub-solar longitude and location of the atmospheric tilt's azimuth orientation relative to this sub-solar longitude.

Image	Time (yyyy,ddd,hh)	Tilt amplitude (degrees latitude)	Tilt azimuth (west longitude)	NSA boundary mean latitude	Sub-solar longitude (W)	Offset west of sub-solar longitude
N1477224220	2004,297,12	4.5 ± 0.4°	140 ± 5°	−7.7 ± 0.6°	89°	51 ± 5°
N1481448770	2004,346,09	5.3 ± 0.7°	158 ± 8°	−7.7 ± 0.8°	110°	48 ± 8°
W1487123242	2005,046,01	3.7 ± 0.3°	261 ± 4°	−12.4 ± 1.2°	151°	110 ± 4°
N1496569460	2005,155,09	3.9 ± 0.5°	167 ± 10°	−7.5 ± 0.7°	95°	72 ± 10°
N1496574260	2005,155,10	3.9 ± 0.5°	165 ± 10°	−7.6 ± 1.1°	96°	69 ± 10°
N1496579060	2005,155,12	3.6 ± 0.5°	167 ± 11°	−7.9 ± 1.5°	97°	70 ± 11°
N1496583860	2005,155,13	3.2 ± 0.3°	177 ± 13°	−9.0 ± 1.5°	99°	78 ± 13°
W1509139296	2005,300,20	4.2 ± 0.3°	196 ± 9°	−7.9 ± 0.5°	147°	49 ± 9°
W1509148861	2005,300,23	3.2 ± 0.1°	225 ± 7°	−9.4 ± 0.5°	136°	89 ± 7°
W1514292901	2005,360,12	2.0 ± 0.3°	83 ± 8°	−7.6 ± 0.5°	38°	45 ± 8°
N1557906451	2007,135,07	4.0 ± 0.5°	335 ± 10°	−9.1 ± 1.1°	257°	78 ± 10°
W1559103294	2007,149,03	4.9 ± 0.1°	300 ± 7°	−9.3 ± 1.0°	209°	91 ± 7°
N1559283948	2007,151,06	2.0 ± 0.2°	35 ± 7°	−9.0 ± 0.7°	257°	138 ± 7°
W1561882135	2007,181,07	4.3 ± 0.2°	301 ± 8°	−7.1 ± 0.6°	215°	86 ± 8°
W1561882245	2007,181,07	4.5 ± 0.5°	296 ± 13°	−7.5 ± 1.4°	215°	81 ± 13°
W1561882355	2007,181,07	4.9 ± 0.7°	288 ± 17°	−5.6 ± 1.5°	215°	73 ± 17°
N1562038525	2007,183,03	4.2 ± 0.5°	305 ± 15°	−6.1 ± 0.8°	255°	50 ± 15°
N1567440863	2007,245,15	3.8 ± 0.1°	318 ± 6°	−8.5 ± 0.3°	225°	93 ± 6°
N1570187018	2007,277,10	3.1 ± 0.2°	322 ± 7°	−9.5 ± 0.5°	221°	101 ± 7°
N1570187128	2007,277,10	2.7 ± 0.2	323 ± 7°	−9.7 ± 0.5	221°	102 ± 7°
Weighted mean		3.8°	228°	−8.4°	167°	85°
Std. deviation		0.9°	89°	1.5°	69°	24°

50 km less than the nominal 80 km height value were tested to estimate the consequent uncertainty in our measurements. Our analysis showed that each of these parameters introduced considerable uncertainty to our values; not surprisingly, measurements of images with relatively low spatial resolution displayed greater sensitivity to the pointing error whereas measurements from higher resolution images were particularly sensitive to changes in the effective radius, which we noted was not well constrained. Furthermore, the goodness of fits to data within the expected range did not clearly indicate which input parameters were superior. The significant error contribution from these seemingly small navigational uncertainties may perhaps be seen as an indication of the subtle ambiguity in the precise location of the contrast boundary.

Uncertainty for each of these parameters was estimated in the manner above and added in quadrature to the previously determined error for that parameter. The result was a calculation of a one-sigma standard deviation uncertainty in our ability to determine the tilt parameters based on the cumulative uncertainty of the data; this is value quoted as the uncertainty in Table 2.

The uncertainties provided are our best attempt to quantify the uncertainty in this difficult measurement; though we have tried to reasonably account for all errors, we feel that the reported uncertainties may still be underestimating the true uncertainty in each measurement. This view is based on the discrepancy in measured values between nearly contemporaneous images. Physical variation between images separated by only a few hours is assumed to be insignificant, and any discrepancy is therefore due to error in our measurements. For example, images W1509139296 and W1509148861 are separated by only 3 h in time, yet they yielded tilt amplitudes of 4.2° and 3.2°, respectively, with error bars of only 0.3° and 0.2°. This suggests that there is still an inherent uncertainty in our measurements that we have failed to accurately quantify. Further such examples can be found our data set. Given this, we feel that the precision of the value and uncertainty of any individual image measurement should be regarded as less significant than the cumulative assertion of the data set, for which mean and standard deviation express a more reliable statement of the desired measurements.

3. Results

For each image, the parameters representing the mean axial offset of the NSA and the implied atmospheric spin have been calculated. The results are presented in Table 2. In this table, the first two columns present the image name along with the time at which it was taken (year, day of the year, hour of the day), respectively. The images are listed in chronological order. The third column reports the magnitude of the offset, in degrees of latitude, of the atmospheric pole with respect to the solid body pole. The fourth column reports the azimuthal orientation of the offset, in degrees

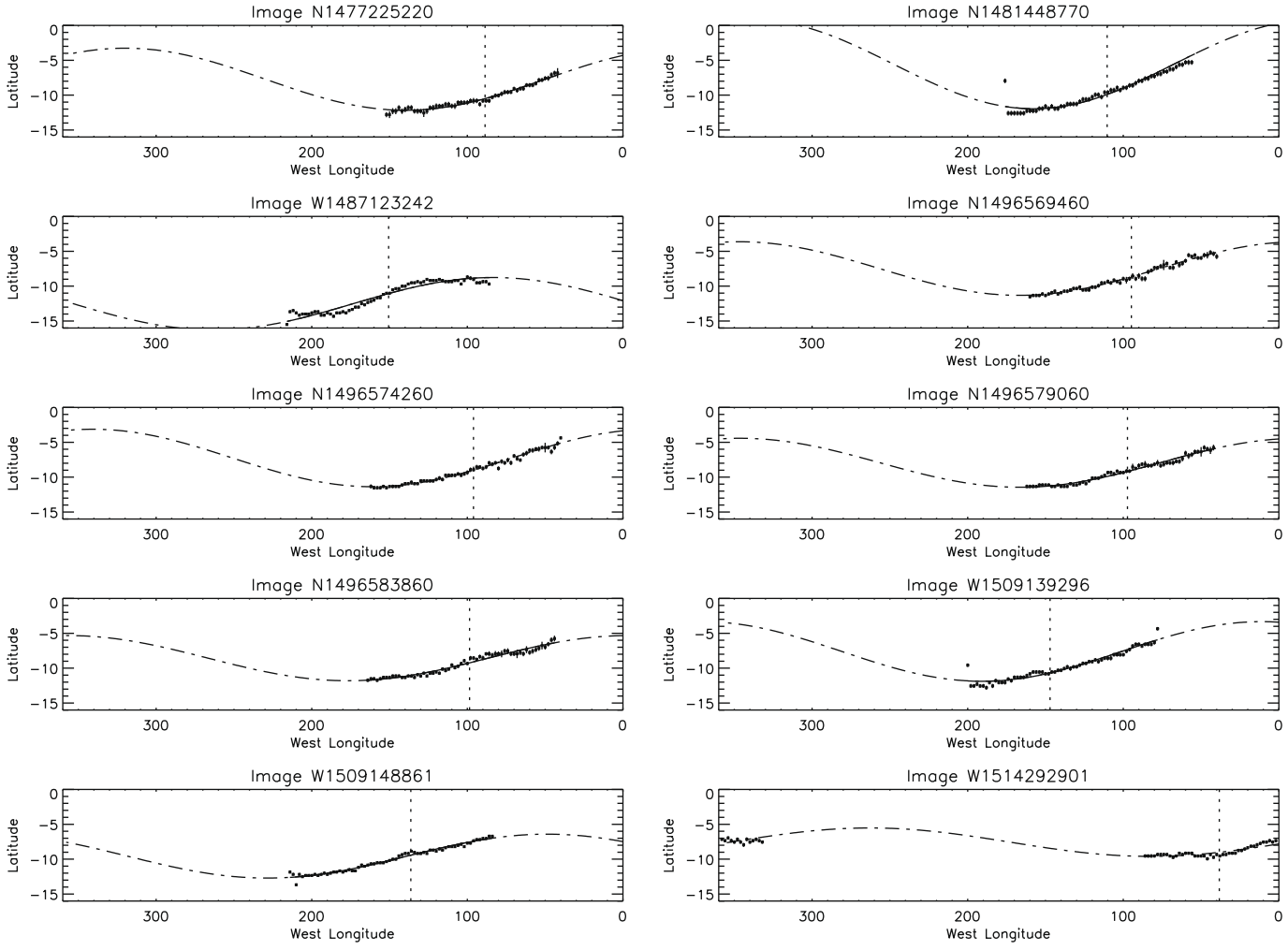

Fig. 7. As in Fig. 6, Plots of the NSA boundary latitude as a function of longitude, with error bars representing the uncertainty of the boundary latitude for each bin of longitudes. The sub-solar longitude is once again represented with a vertical dotted line, with sub-solar latitude represented by a '*' where present.

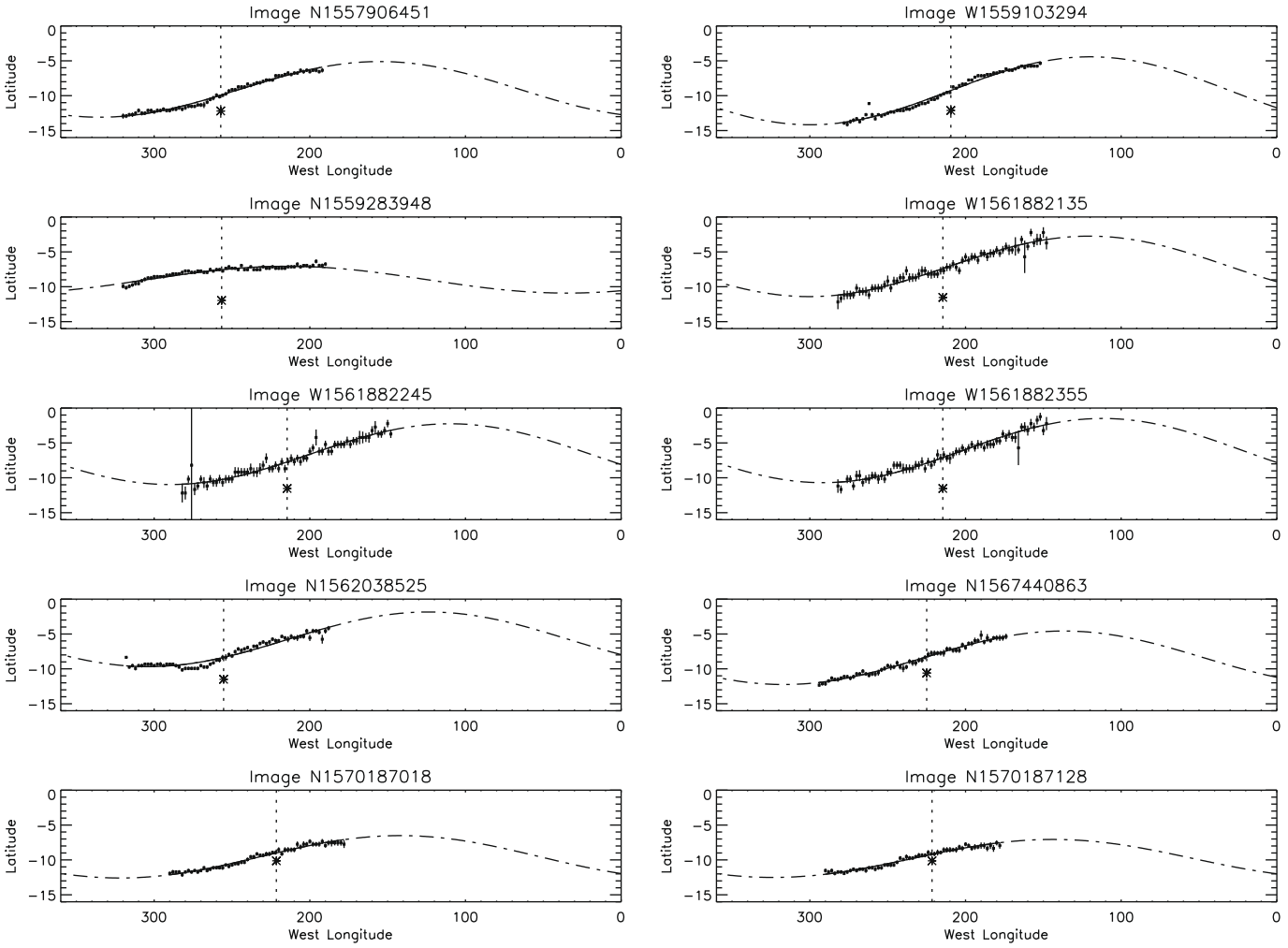

Fig 7. (*continued*)

west longitude, as determined by the phase of the fitted function. The fifth column reports the mean latitude of the NSA boundary as determined by the vertical offset term of the fit. To help reveal possible correlation with insolation, the final two columns provide the sub-solar longitude and location of the atmospheric tilt's azimuth orientation relative to this sub-solar longitude. Corresponding plots of the fitted boundary latitudes as a function of longitude are depicted in Fig. 7.

As noted in our error analysis, there are some discrepancies between nearly contemporaneous images that suggest that the stated uncertainties are likely an underestimate of the true uncertainty in each stated measurement; these uncertainties are nonetheless provided to show the relative uncertainties between images. True uncertainties are estimated to be a factor of two or three larger.

The magnitude of the axial offset for the entire set of images has a mean average of 3.8° of latitude, with a standard deviation of 0.9°. Examination of the tilt azimuth alone reveals a large spread (standard deviation of 89°) with a mean of 228°, but examining tilt azimuths relative to sub-solar longitudes reveals a relatively stronger correlation; the azimuth component of the axial offset when measured in degrees west of sub-solar longitude has a standard deviation of only 24°, with a mean value of 79°. This significantly smaller standard deviation suggests that the azimuth offset is linked to solar heating.

In an attempt to explain the discrepancies between nearly contemporaneous images, we examined the most anomalous pair, *W1559103294* and *N1559283948*, which are separated by only two days, but have tilt amplitudes of 4.9° and 2.0°, respectively. Examination of the images reveals a subtle but noticeable difference in the orientation and shape of the NSA boundary compared to the others. The fit to the NSA boundary does not appear to obviously fail to describe the image data, but the subtlety of the gradient and its measurement make it difficult to determine the accuracy of the fit from simple visual inspection. The value of its reduced chi-square statistic is comparable to that of the other images, and so one may be led to believe that the anomaly may be physical, as perhaps caused by a transient meteorological effect. It should be noted that image *N1559283948* stands out as something of an outlier, for it yielded the greatest azimuth offset relative to sub-solar longitude and shared the smallest tilt. Nonetheless, we could not conclusively account for this discrepancy.

The data set was also examined for temporal variation in the parameters, particularly the azimuth orientation, time evolution of which would have suggested a seasonal dependence. Given the uncertainties in our measurements, we could not determine any clear trend in the results. Analysis of future images would be needed to provide greater temporal resolution before any such conclusions can be made.

4. Conclusion

Given this small set of Cassini image data, the values determined from measuring Titan's north–south albedo asymmetry conclusively indicate a definite axial offset relative to the solid body, measured to be $3.8 \pm 0.9^\circ$ in latitude directed $79 \pm 24^\circ$ to the west of the sub-solar longitude. We interpret this as an approximately 4° tilt in the atmospheric spin axis directed about 5 h west of solar noon. This value is in strong agreement with recent thermally deduced values of $4.1 \pm 0.2^\circ$ directed $76 \pm 2^\circ$ west of sub-solar longitude, as determined by Achterberg et al. (2008b), and may serve as a visual image complement to their CIRS findings. With a clearer characterization of Titan's atmospheric rotation, we can expect to gain a greater understanding of the dynamics of super-rotating atmospheres.

Acknowledgment

The authors acknowledge the support of the NASA Cassini project during the period in which this work was conducted.

References

Achterberg, R.K., Conrath, B.J., Gierasch, P.J., Flasar, F.M., Nixon, C.A., 2008a. Titan's middle-atmospheric temperatures and dynamics observed by the Cassini Composite Infrared Spectrometer. Icarus 194, 263–277.

Achterberg, R.K., Conrath, B.J., Gierasch, P.J., Flasar, F.M., Nixon, C.A., 2008b. Observation of a tilt of Titan's middle-atmospheric super-rotation. Icarus 197, 549–555.

Caldwell, J., Cunningham, C.C., Anthony, D., White, H.P., Groth, E.J., Hasan, H., Noll, K., Smith, P.H., Tomasko, M.G., Weaver, H.A., 1992. Titan: Evidence for seasonal change—A comparison of Hubble space telescope and Voyager images. Icarus 97, 1–9.

Flasar, F.M., Conrath, B.J., 1990. Titan's stratospheric temperatures–A case for dynamical inertia? Icarus 85, 346–354.

Flasar, F.M., Samuelson, R.E., Conrath, B.J., 1981. Titan's atmosphere–Temperature and dynamics. Nature 292, 693–698.

Flasar, F.M., and 44 colleagues, 2004. Exploring the Saturn system in the thermal infrared: The Composite Infrared Spectrometer. Space Sci. Rev. 115, 169–297.

Kostiuk, T., Fast, K.E., Livengood, T.A., Hewagama, T., Goldstein, J.J., Espenak, F., Buhl, D., 2001. Direct measurement of winds on Titan. Geophys. Res. Lett. 28, 2361–2364.

Lorenz, R.D., Smith, P.H., Lemmon, M.T., Karkoschka, E., Lockwood, G.W., Caldwell, J., 1997. Titan's north–south asymmetry from HST and voyager imaging: Comparison with models and ground-based photometry. Icarus 127, 173–189.

Porco, C.C., West, R.A., Squyres, S., Mcewen, A., Thomas, P., Murray, C.D., Delgenio, A., Ingersoll, A.P., Johnson, T.V., Neukum, G., Veverka, J., Dones, L., Brahic, A., Burns, J.A., Haemmerle, V., Knowles, B., Dawson, D., Roatsch, T., Beurle, K., Owen, W., 2004. Cassini imaging science: Instrument characteristics and anticipated scientific investigations at Saturn. Space Sci. Rev. 115, 363–497.

Seidelmann, P.K., Archinal, B.A., A'hearn, M.F., Conrad, A., Consolmagno, G.J., Hestroffer, D., Hilton, J.L., Krasinsky, G.A., Neumann, G., Oberst, J., Stooke, P., Tedesco, E.F., Tholen, D.J., Thomas, P.C., Williams, I.P., 2007. Report of the IAU/IAG working group on cartographic coordinates and rotational elements: 2006. Celestial Mech. Dyn. Astr. 98, 155–180.

Sicardy, B., Ferri, F., Roques, F., Lecacheux, J., Pau, S., Brosch, N., Nevo, Y., Hubbard, W.B., Reitsema, H.J., Blanco, C., Carreira, E., Beisker, W., Bittner, C., Bode, H.-J., Bruns, M., Denzau, H., Nezel, M., Riedel, E., Struckmann, H., Appleby, G., Forrest, R.W., Nicolson, I.K.M., Hollis, A.J., Miles, R., 1999. The structure of Titan's stratosphere from the 28 Sgr occultation. Icarus 142, 357–390.

Smith, B.A., Soderblom, L., Beebe, R., Boyce, J., Briggs, G., Bunker, A., Collins, S.A., Hansen, C.J., Johnson, T.V., Mitchell, J.L., Terrile, R.J., Carr, M., Cook II, A.F., Cuzzi, J., Pollack, J.B., Danielson, G.E., Ingersoll, A., Davies, M.E., Hunt, G.E., Masursky, H., Shoemaker, E., Morrison, D., Owen, T., Sagan, C., Veverka, J., Strom, R., Suomi, V.E., 1981. Encounter with Saturn: Voyager 1 imaging science results. Science 212, 163–191.

Sromovsky, L.A., Suomi, V.E., Pollack, J.B., Krauss, R.J., Limaye, S.S., Owen, T., Revercomb, H.E., Sagan, C., 1981. Implications of Titan's north–south brightness asymmetry. Nature 292, 698–702.

Stiles, B.W., Kirk, R.L., Lorenz, R.D., Hensey, S., Lee, E., Ostro, S.J., Allison, M.D., Callahan, P.S., Yonggyu, G., Iess, L., Del Marmo, P.P., Hamilton, G., Johnson, W.T.K., West, R.D.the Cassini RADAR Team, 2008. Determining Titan's spin state from Cassini radar images. Science 319, 1649–1651.